LHCb Collaboration

LHCb 2007-050
10 March 2007

Estimate of LHCb's sensitivity to the CKM angle γ using $B^0 \rightarrow D^0 K^{*0}$ Decays

K. Akiba, M. Gandelman
IF-UFRJ/Brazil

Abstract

In this note an updated event selection of the $B^0 \rightarrow D^0 K^{*0}$ decay, with the D^0 decaying into $K\pi$, KK, $\pi\pi$ is presented. The selection efficiencies are used to estimate the statistical error for determining the CKM phase γ applying a combination of the GLW and ADS methods.

1 Introduction

This note reports on a Monte Carlo study of the sensitivity of LHCb to the unitarity triangle angle γ with $B^0 \to D^0 K^{*0}$ decays. The selection studies have been performed with the so-called DC04 simulation production. In contrast to the earlier analyses reported in [1, 2], the present study takes full account of the doubly Cabibbo suppressed (DCS) amplitude contributing to the $D \to K\pi$ decay. The results presented in this note supersede those of the previous LHCb studies.

The note is organised as follows. Section 2 explains how $B^0 \to D^0 K^{*0}$ can be used to determine γ, and discusses the contribution of the DCS $K\pi$ amplitude. Section 3 reports on the event selection, and gives the final estimated signal yields and background levels. Section 4 presents the sensitivity studies and resulting γ precision. A summary is given in Section 5.

2 Theory

$B^0 \to D^0 K^{*0}$ decays can be used to extract directly the phase γ of the CKM unitarity triangle. In previous studies (which can be found in [1] and [2]) the effect of DCS decays was neglected for reasons of simplicity. In the present work the interference effects coming from this source are considered.

Let A_1 and A_2 represent the magnitude of the amplitudes for the decays $B^0 \to \overline{D}^0 K^{*0}$ and $B^0 \to D^0 K^{*0}$ respectively. There is a phase difference of $\delta_B + \gamma$ between these two amplitudes, where δ_B is a CP-conserving phase arising from strong interactions between the final state particles (D^0 and K^{*0}). As originally proposed in [3], the effect of this phase difference can be observed by reconstructing the D meson in a final state that is common to both D^0 and $\overline{D}^0$. An interesting example is the case where the final state is a CP eigenstate such as K^+K^- or $\pi^+\pi^-$. Then:

$$\begin{aligned} A(B^0 \to D_{CP}K^{*0}) \equiv A_3 &\propto \frac{1}{\sqrt{2}}[A(B^0 \to \overline{D}^0 K^{*0}) + A(B^0 \to D^0 K^{*0})] \\ &\propto \frac{1}{\sqrt{2}}(A_1 + A_2 e^{i\delta_B} e^{i\gamma}), \end{aligned} \tag{1}$$

where D_{CP} denotes the even CP eigenstate mode, given by $D_{CP} = \frac{1}{\sqrt{2}}(D^0 + \overline{D}^0)$. The decay width for this process will be given by Γ_3, where:

$$\Gamma_3 \propto \Gamma_1 + \Gamma_2 + 2\sqrt{\Gamma_1\Gamma_2}\cos(\delta_B + \gamma). \tag{2}$$

Here Γ_1 and Γ_2 signify the decay widths of $B^0 \to \overline{D}^0 K^{*0}$ and $B^0 \to D^0 K^{*0}$. Using the CP conjugates of the amplitudes of expression 1, the corresponding relation for the $\overline{B}^0$ decay can be written:

$$\begin{aligned} A(\overline{B}^0 \to D_{CP}\overline{K}^{*0}) \equiv A_4 &= \frac{1}{\sqrt{2}}[A(\overline{B}^0 \to D^0\overline{K}^{*0}) + A(\overline{B}^0 \to \overline{D}^0\overline{K}^{*0})] \\ &= \frac{1}{\sqrt{2}}(A_1 + A_2 e^{i\delta_B} e^{-i\gamma}), \end{aligned} \tag{3}$$

and hence the decay width Γ_4 is given by:

$$\Gamma_4 \propto \Gamma_1 + \Gamma_2 + 2\sqrt{\Gamma_1\Gamma_2}\cos(\delta_B - \gamma). \tag{4}$$

Measurement of the relative sizes of the four decay rates Γ_i $(i = 1-4)$ therefore allows γ to be extracted, albeit with discrete ambiguities. An analogous strategy involving charged B decays was initially proposed by Gronau, London and Wyler (GLW) [4].

An experimental challenge with this approach lies in the measurement of Γ_1 and Γ_2. Determining these widths requires the detection of a D final state that is a flavour eigenstate, i.e. a semi-leptonic decay. Isolating a sufficiently pure sample of these decays is a difficult task. More straightforward is to use a near-flavour eigenstate such as $\mathrm{D}^0 \rightarrow \mathrm{K}^-\pi^+$, which is ≈ 200 times more probable than the DCS decay $\mathrm{D}^0 \rightarrow \mathrm{K}^+\pi^-$. The contribution of the DCS amplitude, however, leads to interference effects which cannot be neglected in the analysis.

As both D^0 and $\overline{\mathrm{D}}^0$ can decay into the same $\mathrm{K}^+\pi^-$ final state, the decay amplitude of B^0 into a $(\mathrm{K}^+\pi^-)_\mathrm{D}$ K^{*0} state will be given by:

$$\begin{aligned} A(\mathrm{B}^0 \rightarrow (\mathrm{K}^+\pi^-)_\mathrm{D}\ \mathrm{K}^{*0}) \ \propto\ & A(\mathrm{B}^0 \rightarrow \overline{\mathrm{D}}^0\mathrm{K}^{*0})A(\overline{\mathrm{D}}^0 \rightarrow \mathrm{K}^-\pi^+)e^{i\delta_\mathrm{D}} \\ & + A(\mathrm{B}^0 \rightarrow \mathrm{D}^0\ \mathrm{K}^{*0})A(\mathrm{D}^0 \rightarrow \mathrm{K}^-\pi^+), \end{aligned} \tag{5}$$

where δ_D is introduced to make explicit the possible strong interaction phase difference between the Cabibbo Favoured (CF) and DCS decays. Similarly, one has:

$$\begin{aligned} A(\mathrm{B}^0 \rightarrow (\mathrm{K}^-\pi^+)_\mathrm{D}\ \mathrm{K}^{*0}) \ \propto\ & A(\mathrm{B}^0 \rightarrow \overline{\mathrm{D}}^0\mathrm{K}^{*0})A(\overline{\mathrm{D}}^0 \rightarrow \mathrm{K}^+\pi^-) \\ & + A(\mathrm{B}^0 \rightarrow \mathrm{D}^0\ \mathrm{K}^{*0})A(\mathrm{D}^0 \rightarrow \mathrm{K}^+\pi^-)e^{i\delta_\mathrm{D}}, \end{aligned} \tag{6}$$

and equivalent expressions for the two $\overline{\mathrm{B}^0}$ decay modes.

It is useful to define the following ratios:

$$\mathrm{r_B} \equiv \frac{\mathrm{A_2}}{\mathrm{A_1}} = \frac{|\mathrm{A}(\mathrm{B}^0 \rightarrow \mathrm{D}^0\ \mathrm{K}^{*0})|}{|\mathrm{A}(\mathrm{B}^0 \rightarrow \overline{\mathrm{D}}^0\mathrm{K}^{*0})|} \tag{7}$$

and

$$\mathrm{r_D} \equiv \frac{|\mathrm{A}(\mathrm{D}^0 \rightarrow \mathrm{K}^+\pi^-)|}{|\mathrm{A}(\overline{\mathrm{D}}^0 \rightarrow \mathrm{K}^+\pi^-)|}. \tag{8}$$

The factor $\mathrm{r_D}$[1] is well measured and has a value of 0.06 ± 0.003 [5]. $\mathrm{r_B}$ is yet unknown, but, as explained in Section 4, it is expected to have a value of ~ 0.4, which is significantly larger than the analogous parameter in the $\mathrm{B}^\pm$ system.

Using this notation, the decay widths of the four decay modes involving $\mathrm{K}\pi$ are given by:

$$\Gamma(\mathrm{B}^0 \rightarrow (\mathrm{K}^+\pi^-)_\mathrm{D}\mathrm{K}^{*0}) \ \propto\ 1 + (\mathrm{r_B r_D})^2 + 2\mathrm{r_B r_D}\cos(\delta_\mathrm{B} + \delta_\mathrm{D} + \gamma), \tag{9}$$

$$\Gamma(\mathrm{B}^0 \rightarrow (\mathrm{K}^-\pi^+)_\mathrm{D}\mathrm{K}^{*0}) \ \propto\ \mathrm{r_B}^2 + \mathrm{r_D}^2 + 2\mathrm{r_B r_D}\cos(\delta_\mathrm{B} - \delta_\mathrm{D} + \gamma), \tag{10}$$

$$\Gamma(\overline{\mathrm{B}}^0 \rightarrow (\mathrm{K}^-\pi^+)_\mathrm{D}\overline{\mathrm{K}}^{*0}) \ \propto\ 1 + (\mathrm{r_B r_D})^2 + 2\mathrm{r_B r_D}\cos(\delta_\mathrm{B} + \delta_\mathrm{D} - \gamma), \tag{11}$$

$$\Gamma(\overline{\mathrm{B}}^0 \rightarrow (\mathrm{K}^+\pi^-)_\mathrm{D}\overline{\mathrm{K}}^{*0}) \ \propto\ \mathrm{r_B}^2 + \mathrm{r_D}^2 + 2\mathrm{r_B r_D}\cos(\delta_\mathrm{B} - \delta_\mathrm{D} - \gamma), \tag{12}$$

where the constant of proportionality is the same for each decay. Similarly, the widths for the two modes involving the $\mathrm{D_{CP}}$ can be written as:

$$\Gamma(\mathrm{B}^0 \rightarrow \mathrm{D_{CP}K}^{*0}) \ \propto\ 1 + \mathrm{r_B}^2 + 2\mathrm{r_B}\cos(\delta_\mathrm{B} + \gamma), \tag{13}$$

$$\Gamma(\overline{\mathrm{B}}^0 \rightarrow \mathrm{D_{CP}}\overline{\mathrm{K}}^{*0}) \ \propto\ 1 + \mathrm{r_B}^2 + 2\mathrm{r_B}\cos(\delta_\mathrm{B} - \gamma), \tag{14}$$

[1] PDG defines $\mathrm{r_D}$ in terms of the relative branching ratios, that is equivalent to a value around 0.0036. We prefer to use the convention of expression 8, in order to maintain uniformity with the definition of $\mathrm{r_B}$.

introducing two new equations and only one new parameter, hidden in the proportionality constant.

Therefore measuring all six decay rates allows the four unknowns of interest, γ, δ_B, δ_D and r_B, to be determined. The interference terms in expressions 9 to 12 were ignored in the previous LHCb studies [1, 2]. For the equivalent expressions in the $B^{\pm}$ system, where $r_B \sim r_D$, these interference terms enter at first order for two of the rates and hence give significant additional sensitivity to γ. This feature was pointed out by Atwood, Dunietz and Soni (ADS) in [6]. In the B^0 system, where $r_B >> r_D$, this is not the case. Nevertheless, as will be shown, it is important to take account of this interference to not introduce a significant bias in the γ extraction.

Finally, it can be noted that an ADS-like analysis of $B^0 \rightarrow D^0 K^{*0}$ decays will benefit from studies of coherent D production at CLEO-c and BES III, which will introduce constraints on the value of $\cos(\delta_D)$.

3 Event Selection

The selection of the signal channels is described in the following sections. The general philosophy is based on the approach described in [1] and [2]. The total yield will then be estimated based on the efficiency of this selection. Three different signal channels were analysed, and a common background sample was used to estimate the background levels. The LHCb analysis package DaVinci [7] was used to analyse the simulated data and generate ntuples that were analysed further with ROOT [8]. Both the signal and the background were generated with the LHCb Data Challenge 2004 (DC04) settings. The background analysed here, however, comes from a second batch of this generation – the so-called DC04v2 data set. This data sample is constituted of about 34 million events containing a $b\overline{b}$ quark pair produced inside the angular acceptance of the LHCb detector, decaying inclusively.

3.1 Selection Sequence

The event selection is structured on three consecutive algorithms operating on reconstructed signal tracks and fitted vertices. In this sequence of algorithms the first one attempts to find a D^0 in any of the final states of interest ($D^0 \rightarrow K^-\pi^+$, $D^0 \rightarrow \pi^+\pi^-$, $D^0 \rightarrow K^+K^-$). If at least one D^0 is found the sequence proceeds in trying to reconstruct a K^{*0} vertex in the charged $K^+\pi^-$ final state. If both conditions are satisfied, which means that in a particular event a D^0 and a K^{*0} are found, the third algorithm is called. This algorithm attempts to use the four selected tracks to reconstruct a B^0 vertex with the topology of $B^0 \rightarrow D^0 K^{*0}$. The specific conditions to accept or to reject each candidate are described in the following sections.

3.2 D^0 Selection

The D^0 selection is performed by fitting a vertex to any combination of K and π that satisfy basic requirements on impact parameter significance (IPS) with respect to the primary vertex (PV), and transverse momentum (P_T). Later on, the reconstructed B^0 will rely on the particle identification to separate the different decay types of the D^0.

h minimum P_T	300 MeV/c
h minimum momentum	2000 MeV/c
h minimum IPS	2.0
D^0 minimum P_T	1000 MeV/c
D^0 mass window	$\pm$ 20 MeV/c^2
D^0 vertex maximum χ^2/ndof	25
D^0 vertex maximum mass constrained χ^2/ndof	25

Table 1: List of cuts applied in the D^0 selection; h refers to either K or π.

h minimum P_T	200 MeV/c
h minimum momentum	2000 MeV/c
h minimum IPS	2.0
K^{*0} minimum P_T	500 MeV/c
K^{*0} mass window	$\pm$ 150 MeV/c^2
K^{*0} vertex maximum χ^2/ndof	25

Table 2: List of cuts applied in the K^{*0} selection; h refers to either K or π.

There is no dedicated MC sample of DCS $D^0 \rightarrow K^+\pi^-$ decays available . It is assumed that the reconstruction performance is identical to the CF mode $D^0 \rightarrow K^-\pi^+$.

The list of requirements for a D^0 candidate to be accepted is shown in Table 1.

3.3 K^{*0} Selection

The selection of a K^{*0} candidate follows the same overall condition as for the D^0 candidates but with slightly different criteria, since the K^{*0} is a broader resonance. The specific list of cuts for this preselection is shown in Table 2.

3.4 B^0 Pre-selection

In building up the B^0 candidate, conditions are placed on: the P_T and IPS of the previously selected D^0 and K^{*0} candidates; the quality of the B^0 vertex; the IPS of the B^0; the consistency of the B^0 flight direction with the interaction point; and two event variables quantifying the P_T and IPS of all the contributing tracks. These cuts are listed in Table 3 and constitute the B^0 pre-selection. In addition to these requirements a discrete selection criterion is imposed termed the 'vertex isolation cut', which seeks to further suppress combinatoric background by rejecting events where there is evidence of other tracks being associated with the B^0 decay vertex.

The vertex isolation criterion was tested in two distinct configurations, which are not completely uncorrelated:

- first, removing events with 4 or more particles, in addition to the candidate B^0 decay tracks, pointing to the B^0 vertex with IPS smaller than 2.0;

D^0 or K^{*0} minimum P_T	1000 MeV/c
D^0 or K^{*0} minimum IPS	2.0
B^0 mass window	$\pm$ 500 MeV/c^2
B^0 vertex maximum χ^2/ndof	25
B^0 maximum IPS	5.0
B^0 momentum·flight vector	> 0.999
Minimum $\Sigma \log(h_{P_T})$	25.0
Minimum $\Sigma \log(h_{IPS})$	5.5

Table 3: List of cuts applied in the B^0 pre-selection. In addition to these requirements a vertex isolation cut is imposed (see text).

- second, removing those events with at least 1 particle, in addition to the candidate B^0 decay tracks, pointing to the reconstructed B^0 vertex with an IPS smaller than 1.0.

The second approach was found to be more effective in suppressing background events coming from random sources and coming from specific final states such as $D^{*+} \to D^0\pi^+$ or $D_s \to D^0K$.

3.5 B^0 Final Selection

In order to suppress the background to an acceptable level it is necessary to make a final selection involving both tighter versions of the existing cuts, and the introduction of certain new requirements. Due to the distinct nature of the D^0 hadronic final states, the rate of reconstructed background based on random combinatoric events can be different from channel to channel and hence channel specific selections may be appropriate. The final set of cuts are listed in Table 4. Discussion of each cut variable can be found in [1] and [2].

In Figure 1 the mass distributions for the reconstructed B^0 after all requirements apart from the the tight mass window cut are plotted. The combinatoric background from the signal sample is low and therefore neglected in any further background estimates.

3.6 Event Yields and Efficiencies

The total efficiency $\varepsilon_{\rm tot}$ is computed as the fraction of MC events containing a signal B^0 that is triggered, reconstructed and selected. It is given by:

$$\varepsilon_{\rm tot} = \varepsilon_{\rm det} \times \varepsilon_{\rm rec/det} \times \varepsilon_{\rm sel/rec} \times \varepsilon_{\rm trg/sel}\,, \tag{15}$$

where $\varepsilon_{\rm det}$ is the detection efficiency, including the geometrical acceptance, $\varepsilon_{\rm rec/det}$ is the reconstruction efficiency on detected events, $\varepsilon_{\rm sel/rec}$ is the offline selection efficiency, and $\varepsilon_{\rm trg/sel}$ is the efficiency of both L0 and L1 triggers on the offline-selected events. The signal retention for these two levels of trigger applied consecutively is around 50%. The High Level Trigger (HLT) efficiency has not been included, but is is expected not to reduce the signal efficiency significantly. The resulting final efficiencies can be found in Table 5.

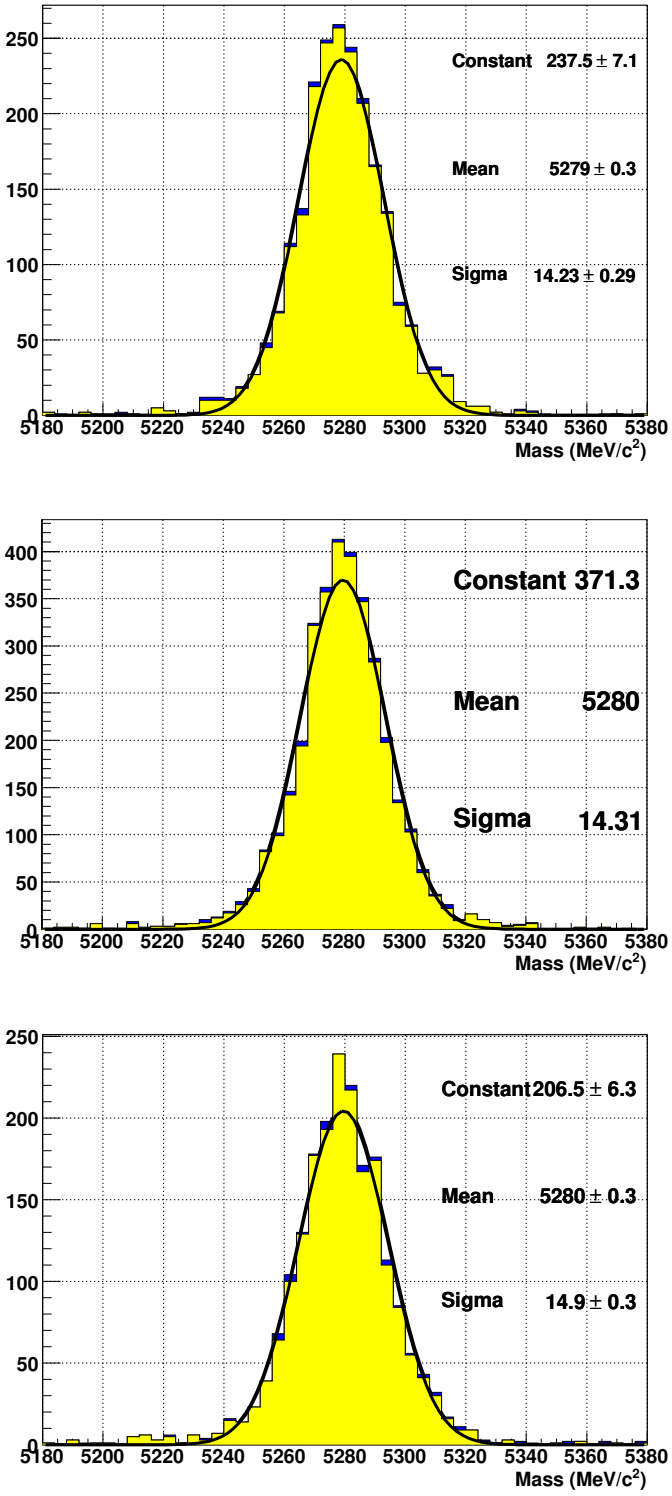

Figure 1: Mass distributions for $B^0 \rightarrow D^0(K^+\pi^-)K^{*0}$, $B^0 \rightarrow D_{CP}(K^+K^-)K^{*0}$ and $B^0 \rightarrow D_{CP}(\pi^+\pi^-)K^{*0}$, from top to bottom respectively. The yellow (pale) histogram shows the events passing the selection which are associated to a genuine $B^0 \rightarrow D^0\ K^{*0}$ decay. The blue (dark) entries correspond to background and unassociated events reconstructed on the signal tapes.

	$D^0 \to K^-\pi^+$	$D^0 \to K^+K^-$	$D^0 \to \pi^+\pi^-$
D^0 vertex maximum χ^2/ndof	20	12	20
K^{*0} vertex maximum χ^2/ndof	20	20	20
B^0 vertex maximum χ^2/ndof	20	20	20
Maximum IPS of D^0 wrt K^{*0} vertex	5	5	3
D^0 or K^{*0} minimum P_T	1000 MeV/c	1000 MeV/c	1000 MeV/c
D^0 or K^{*0} minimum IPS	2.0	2.0	2.0
Maximum B^0 IPS wrt PV	3.0	3.0	3.0
Maximum final state h P_T	300 MeV/c	300 MeV/c	300 MeV/c
B^0 momentum·flight vector	> 0.9990	> 0.9990	>0.9999
Minimum $\Sigma \log(h_{P_T})$	29.0	27.5	29.0
Minimum $\Sigma \log(h_{IPS})$	6.0	6.0	6.0
Minimum $\frac{D^0_{vtx}(z) - B^0_{vtx}(z)}{\sigma}$	0.0	0.0	0.6
Maximum K (from K^{*0}) momentum	90 GeV/c	-	-

Table 4: Summary list of the final cuts applied to each analysed channel.

In addition, Table 5 shows the total number of events expected to be seen for each decay channel in one year of data taking, which corresponds to 2 fb^{-1} of integrated luminosity. The B/S ratios also listed here were calculated using the expected event yield and background limits after the trigger algorithms. For the CKM suppressed mode, $B^0 \to D^0(K^+\pi^-)K^{*0}$, the signal yield (also quoted in Table 5) is assumed to be a factor $r_B{}^2$ smaller than the favoured mode. Here r_B is taken to be 0.4. The background levels are also assumed to be the same as for the $B^0 \to D^0(K^+\pi^-)K^{*0}$ case. Since the number of events for the CP eigenstates modes depends strongly on the phases, the values of δ_B and γ have to be defined. For the entries in this table the phases were assumed to be 0, which implies no CP violation.

3.7 Background Sources

34 million events were analysed from the $b\overline{b}$ inclusive sample, corresponding to approximately 15 minutes of data taking. In each mode very few (if any) background events survived the final cuts in a wide mass window (± 500 MeV/c^2 around the B^0 mass). In the case of $D^0 \to K^+K^-$ or $D^0 \to \pi^+\pi^-$ there were no events found.

A total of 17 candidates were found in the wide mass window passing the $B^0 \to D^0\,K^{*0}$ selection (in the $D^0 \to K^-\pi^+$ case), with no restriction placed on the upper momentum of the kaon from the K^{*0} candidate. All of these candidates were made from a genuine D^0, either coming directly from a B hadron, or from an intermediate D^* resonance, itself from a B.

A significant fraction of the surviving background contained fake K^{*0} candidates arising through the misidentification of a pion as a kaon. Many of the incorrect K^{*0} were in fact $\rho \to \pi\pi$ decays. The inclusion of an upper momentum cut of 90 GeV/c on the kaon candidates restricts the kinematical range to that where the RICH provides good pion-kaon discrimination, and reduces the number of background events in the wide mass window to 8, for minimal loss of signal.

Of the remaining 8 candidates, 3 were found to come from $B^0_s \to D^{0*}(D^0)K^{*0}$ decays,

Channel	$\varepsilon_{\rm tot}$ (%)	yield nominal year (2 fb^{-1})	B/S (90%CL)
$B^0 \to \overline{D}^0(K^+\pi^-)K^{*0}$	0.326(11)	3350(11)	[0.35, 2.04]
$B^0 \to D^0(K^+\pi^-)K^{*0}$	-	536(2)	[2.2, 12.8]
$B^0 \to D_{CP}(K^+K^-)K^{*0}$	0.456(13)	474(13)	[0, 4.09]
$B^0 \to D_{CP}(\pi^+\pi^-)K^{*0}$	0.362(12)	134(5)	[0, 14]

Table 5: This table shows the total efficiency of LHCb to reconstruct each decay channel listed, taking into account the trigger algorithms and the offline selection efficiency. It also shows the number of expected events in one year of data taking and the background levels (quoted as B/S ratios). The event yields have been calculated from the branching ratios found in [5] and [9]. The errors and ranges come from the statistical uncertainty of the Monte Carlo data samples. For the signal results it is assumed that the strong and weak phases are equal to 0, and $r_B = 0.4$.

where the photon or π^0 from the D^* was not identified. As these events always fall in mass below the tight signal window, they are not considered as a background component in the analysis. The other 5 candidates were assumed to be representative of background uniformly distributed across the wide mass window, leading to an estimate of 20 times less in the signal window.

These results were used to calculate the expected B/S ranges shown in Table 5.

Additional contamination may arise from $c\overline{c}$ events. This question cannot be studied in a meaningful way with the present Monte Carlo statistics.

4 Sensitivity Studies

Expressions 9 to 14 relate 6 observables to six different parameters: γ, δ_B, δ_D, r_B, r_D and an overall normalization factor which will be termed N_B. (In principle the set of expressions associated with each D decay mode have their own normalization factors, but the ratios of these factors are fixed by the relative D branching ratios and the relative reconstruction efficiencies – it is here assumed that the uncertainties associated with these factors can be neglected.)

In the studies presented here r_D is taken as known ($r_D = 0.060 \pm 0.003$ [5]); its uncertainty has negligible impact on the γ extraction. External constraints are assumed for the parameter δ_D: $\cos(\delta_D)$ is assumed to be known with an accuracy of $\pm 10\%$, following what is expected from measurements of coherent D production by CLEO-c [10]. Here a central value of $\delta_D = 3\,^\circ$ is taken, following the measurements reported in [12].

In the following sensitivity studies a scan over several different values of the parameters γ, δ_B, δ_D and r_B are performed.

In this note the value of r_B is generally assumed to be 0.4. This is justified by the following arguments:

- Firstly, as quoted in [13], the existing measurement of r_B for the charged $B^+ \to D^0K^{*+}$ channel is 0.15 ± 0.09. This low value is consistent with the expectation that the CKM suppressed channel is further inhibited through colour suppression. In the

neutral B meson case, both amplitudes are colour suppressed, hence leading to the expectation that r_B should be ~ 0.45.

- Secondly, calculating directly from the CKM elements one has:

$$r_B = \frac{V_{ub}V_{cs}}{V_{cb}V_{us}} \times (\text{colour factor}). \tag{16}$$

  Considering that the colour factor in the neutral case is around 1 (as opposed to the charged case which is around $\frac{1}{3}$), this results in a r_B value equal to 0.434, according to the most recent measurements of CKM elements magnitudes taken from [5].

- Current direct measurements are not inconsistent with $r_B = 0.4$. The latest results [9] set an upper limit to the BR for the CKM suppressed mode to be smaller than 1.1×10^{-5} (90%CL) and the favoured mode has been measured to have a branching fraction of $(4.0 \pm 0.7) \times 10^{-5}$. This sets a loose upper limit on r_B of 0.5.

A toy Monte Carlo method, similar to the one presented in [11], is used to generate event rates for one nominal year of data taking.

The expected signal event yield for each of the channels are calculated according to the chosen value of the parameters of interest, and the selection efficiencies from Section 3. The absolute background contribution is set to half the upper limit stated in Table 5, i.e. approximately 850 events for each of the 4 modes involving $D^0 \to K^-\pi^+$ and 500 events for each of the 2 modes involving $D^0 \to K^+K^-$ or $D^0 \to \pi^+\pi^-$.

The number of events are then smeared according to the expected statistical fluctuation and a fit is performed to re-extract the parameters of interest. This procedure is repeated 1000 times to give well populated distributions. The mean fit values and their associated errors are determined by fitting a single Gaussian to these distributions. Typically the statistical error of the mean values obtained from the fit to the distributions is 0.4° for the phases, and 0.1% for r_B. The statistical uncertainty on the widths is about 0.3° for the phases and 0.05% for r_B. In the cases where the Gaussian is not an appropriate function to describe the distribution, the value of the RMS is quoted for the error.

The number of reconstructed events changes according to the strong and weak phase difference. To illustrate this variation, Table 6 gives some examples of different annual yield values for some different strong phase δ_B values, but keeping the same weak phase γ and the strong phase δ_D.

Examples of the distributions obtained can be found in Figures 2 and 3. In the plots shown in Figure 2 distributions for a scenario in which the chosen phases give well behaved distributions can be seen. In this case the fit returns results close to the input values given to the simulation.

In Figure 3 the same distributions are shown for a possibly pathological scenario. For certain values of the phases, the spread of fit results is non-Gaussian and biases are seen in the returned value of γ. These features are associated with the presence of close-lying ambiguities or other local minima. (In the analysis of the real data, plots of likelihood contours for the parameters of interest would make clear whether such a situation was occurring.) In these cases, an external condition either on the strong phase or on the value of r_B would be required in order to resolve the ambiguities. Such input would naturally come from the inclusion of other D^0 decay modes, such as $K^0_s\pi^+\pi^-$.

δ_B			0°	10°	20°	30°	40°
B^0	$\rightarrow$	$D^0(K^+\pi^-)K^{*0}$	1712	1724	1735	1743	1750
B^0	$\rightarrow$	$D^0(K^-\pi^+)K^{*0}$	318	329	338	346	351
$\overline{B}^0$	$\rightarrow$	$D^0(K^-\pi^+)\overline{K}^{*0}$	1719	1707	1694	1680	1666
$\overline{B}^0$	$\rightarrow$	$D^0(K^+\pi^-)\overline{K}^{*0}$	310	298	284	270	256
B^0	$\rightarrow$	$D_{CP}(hh)K^{*0}$	474	435	394	352	310
$\overline{B}^0$	$\rightarrow$	$D_{CP}(hh)\overline{K}^{*0}$	474	508	538	562	580

Table 6: The number of events expected in one year of data taking is listed for each of the channels as a function of the strong phase δ_B. $D_{CP}(hh)$ consists of the summed contributions from $D_{CP}(K^+K^-)$ and $D_{CP}(\pi^+\pi^-)$.

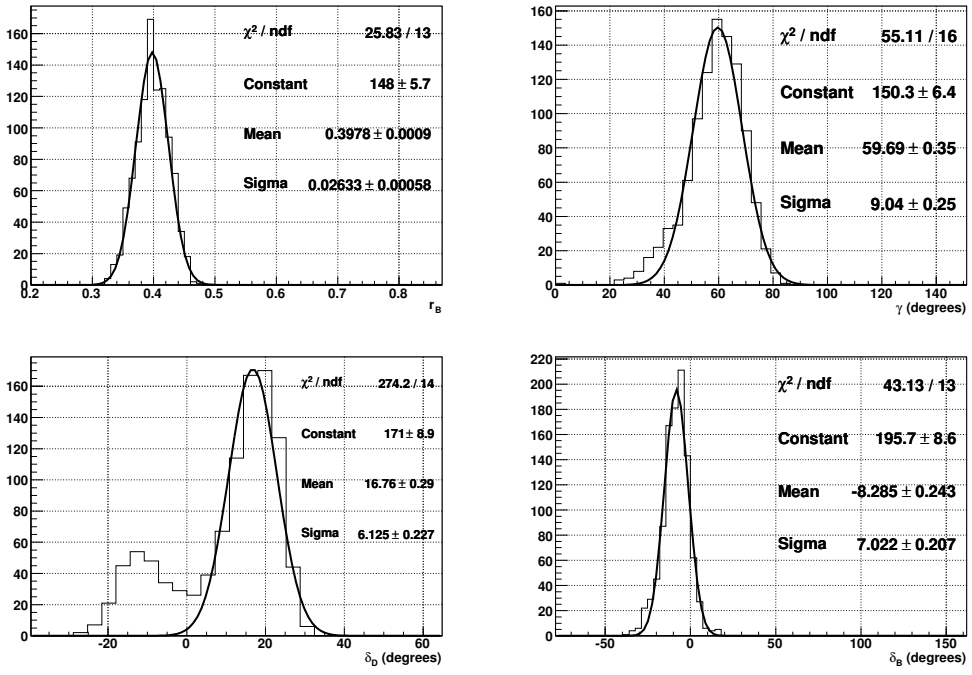

Figure 2: Typical distributions for a well behaved scenario where the fit returns the right values. In this case, the input values were $r_B = 0.4$, $\delta_D = 12^\circ$, $\delta_B = 10^\circ$ and $\gamma = 60^\circ$.

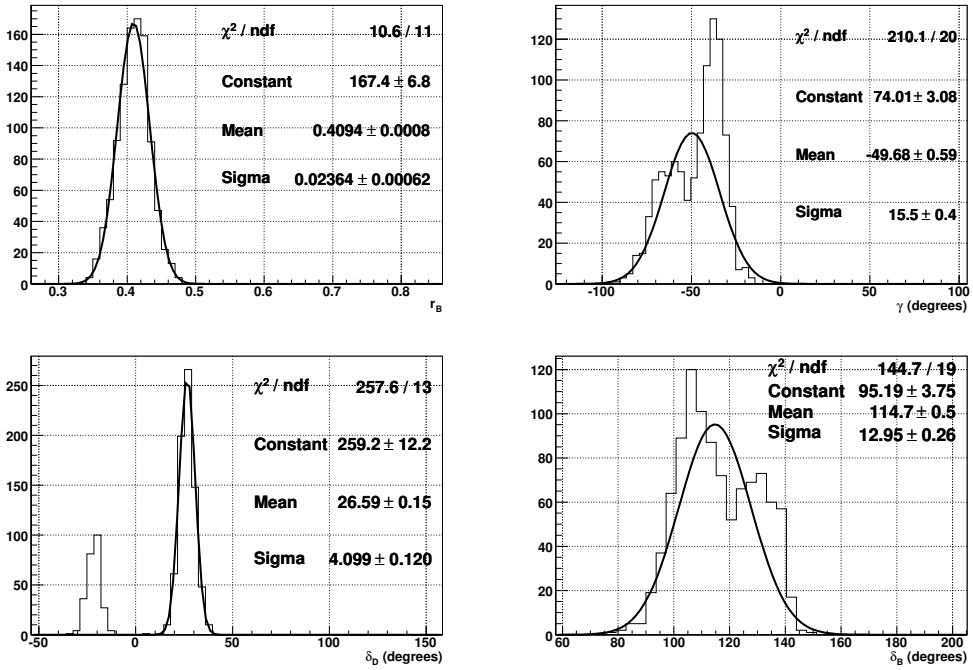

Figure 3: Typical distributions for a badly behaved scenario. The fit returns wrong values or an ambiguous solution. In this case, the input values were $r_B = 0.4$, $\delta_D = 3°$, $\delta_B = 120°$ and $\gamma = 60°$.

In some cases the fit procedure returns an ambiguous solution for one or more phases, δ_B, δ_D, or even γ (as one can conclude from the Figures 2 and 3). There is no obvious explanation for such behavior except that the ambiguous solutions show as a better minimum than the input values. The guessed initial values for the fit routine are the input values to the fast simulation. This could lead to a bias towards to the right solution, however, since the uncertainties are large and the background levels are probably overestimated, the fluctuations are also large and allow ambiguous solutions to appear as central values. The external constraint on the cosine of δ_D can limit the number of possible solutions as well since that constraint limits the phase space of the solutions, which can also lead to fake solutions in the fit.

Table 7 reports the results of a scan through several different values of the strong phase δ_B. It can be seen that the sensitivity has a significant dependence on the value of this parameter. Also note that for certain values of δ_B, the fit does not return the input value for γ. This feature comes about for the reasons discussed in relation to Figure 3.

The variation of the fit results for γ on the variation of the phase δ_D is shown in Table 8. In the range considered little dependence is observed.

In Table 9 the expected precision is shown as a function of γ, around the value of γ predicted by the latest measurements and fits (which can be found in [13]). In Table 9 the column marked 'GLW' shows the values obtained if only a GLW-like analysis is performed on the fast simulation data. By this it is meant that the interference terms from the DCS amplitude are ignored in the γ extraction. It can be seen that this simplification results in a bias on γ which varies in the range $1 - 13°$. (This approximation was used in [1] and

δ_B	$\sigma(\gamma)$	fitted γ
-180°	6.4°	60.3°
-120°	–	-51.3°
-90°	–	-41.1°
-60°	–	-53.0°
-30°	9.6°	60.9°
-20°	8.9°	60.4°
-10°	8.7°	59.4°
0°	8.7°	59.4°
10°	8.8°	59.8°
20°	8.9°	60.6°
30°	9.9°	60.7°
60°	–	-63.0°
90°	–	-40.5°
120°	–	-52.7°
180°	6.4°	60.3°

Table 7: A summary of the results for the fitted γ value and the expected uncertainty based on the obtained distributions, for different values of δ_B. The hyphen(–) indicates the cases where the γ distributions are not Gaussian and the extracted value does not corresponds to the input of the simulation. The input values used in these simulations are $\delta_D = 3°$, $\gamma = 60°$ and $r_B = 0.4$.

δ_D	$\sigma(\gamma)$	fitted γ
-30°	8.7°	59.5°
-18°	8.8°	59.7°
-12°	8.8°	59.7°
-5°	8.8°	59.8°
0°	8.7°	59.8°
5°	8.8°	59.7°
12°	8.7°	59.6°
18°	8.7°	59.7°
30°	8.5°	59.7°

Table 8: A summary for the fitted γ value and the expected uncertainty for a range of values of δ_D. For these results the value of δ_B was fixed to 10°. The input value of γ was 60° and the r_B ratio was 0.4.

[2], but in that case the DCS amplitude was also neglected in the generation phase, and hence no systematic bias was apparent.)

Since r_B has not yet been directly measured, studies have been made of the effect of changing the value of this parameter in the fast simulation. The results, shown in Table 10, indicate that varying this parameter has a significant effect on the uncertainty on γ.

Figure 4 shows how the precision on γ changes for different values of the background

γ	$\sigma(\gamma)$	fitted γ	GLW fitted γ
40°	12.0°	39.5°	53.3°
50°	10.3°	49.5°	59.3°
60°	8.8°	59.7°	66.3°
70°	7.8°	69.6°	73.3°
80°	7.0°	79.6°	81.2°
90°	6.7°	89.5°	89.9°
100°	6.3°	99.5°	98.8°

Table 9: This table shows the error on γ as a function of γ. It also shows a comparison of the mean value obtained with the GLW method alone, where a systematic bias on the γ determination is apparent. For these results the value of $\delta_{\rm B}$ was fixed to 10°, $\delta_{\rm D}$ to 3 ° and the $r_{\rm B}$ ratio to 0.4.

$r_{\rm B}$	$\sigma(\gamma)$	fitted γ
0.1	25°	62.7°
0.2	18°	58.0°
0.3	11.4°	59.4°
0.4	8.7°	59.8°
0.5	7.2°	59.8°
0.6	6.2°	59.9°

Table 10: This table shows how the precision on γ varies with the ratio between the CKM favoured and suppressed channels, $r_{\rm B}$. In this case, the input values of $\delta_{\rm B}$ was fixed to 10°, $\delta_{\rm D}$ to 3° and γ to 60°.

levels. The statistical precision on γ degrades significantly as the background contamination increases.

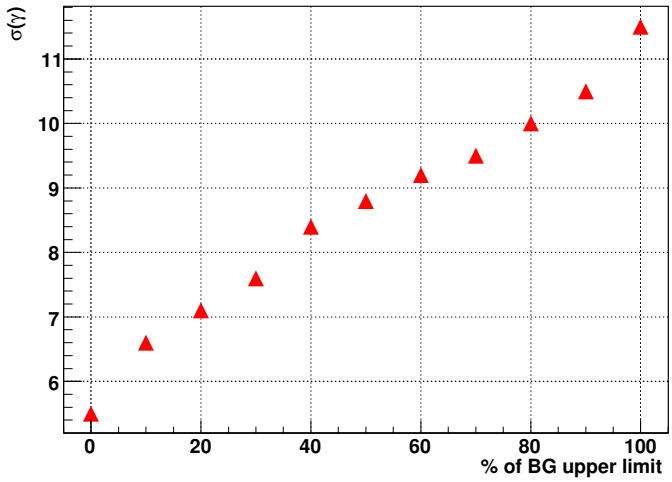

Figure 4: Results for the precision on γ (vertical axis) when varying the background levels (from 0 to 100% of the upper limit, on the horizontal axis). The input values that give these results are $r_B = 0.4$, $\delta_D = 3°$, $\delta_B = 10$ ° and $\gamma = 60$ °.

5 Summary

The studies presented here, based on DC04 simulated data, indicate that $B^0 \rightarrow D^0 K^{*0}$ is a very promising channel for the determination of γ at LHCb. With 2 fb^{-1} of integrated luminosity it is expected that the experiment will accumulate around 3.8k $B^0 \rightarrow D^0 K^{*0}$ events, summed over the four possible flavour combinations. For the CP eigenstate channels, it is expected that around 600 events will be accumulated, where these numbers are quoted neglecting the interference effects, since the contributing phases are unknown at present.

Using these event yields a sensitivity study has been performed, which shows that the expected precision on γ is approximately 9 degrees, for a value of $r_B = 0.40$ and for the level of background indicated by the DC04 analysis. The correct treatment of the DCS amplitudes avoids systematic biases due to the interference effects that were not taken into account in earlier studies.

Additional work is needed to evaluate the systematical uncertainties contributing to the measurement, particularly that associated with additional amplitudes contributing to the K^{*0} resonance. An analysis of the contributing resonances in the $K^+\pi^-$ sector could be included for a more complete γ determination, as proposed in [14].

6 Acknowledgments

We would like to thank Guy Wilkinson for the discussions and the suggestion to use the ADS method in this work.

This work was partially supported by the HELEN project and the Brazilian funding agencies CNPq, FINEP, FUJB and FAPERJ.

References

[1] γ sensitivity with $B^0 \rightarrow D^0 K^{*0}$, K. Akiba, M. Gandelman, LHCb-2003-105, 21 Oct 2003.

[2] Update on γ sensitivity with $B^0 \rightarrow D^0 K^{*0}$, K.Akiba, M. Gandelman. LHCb-2004-045; 24 May 2004.

[3] I.Dunietz, Phys.Lett.B 270(1991)75.

[4] Gronau and London, Phys. Lett. B253, 483 (1991); Gronau and Wyler, Phys.Lett. B265, 172 (1991).

[5] Particle Data Group, W.-M. Yao et al, Journal of physics G 33. 1 (2006).

[6] Atwood, Dunietz, Soni, Phys. Rev. Lett. 78 3257 (1997) .

[7] DaVinci: The LHCb Analysis Program, http://lhcb-release-area.web.cern.ch/LHCb-release-area/DOC/davinci/

[8] ROOT An object oriented data analysis framework http://root.cern.ch/

[9] Measurement of $\overline{B}^0 \rightarrow D^{0(*)}\overline{K}^{*0}$ Branching Fractions. BABAR-PUB-06002. SLAC-PUB-11806.

[10] A projected error of ± 0.05 is quoted for $\cos(\delta_D)$ in the talk of David Asner at CKM 2005. See Asner, 'Experimental Input from CLEO-C', March 18 WG5 Session 5 presentation at 'CKM 2005 Workshop', San Diego, USA.

[11] Measuring γ at LHCb in $B^- \rightarrow D^0 K^-$ decays with an ADS method , G. Wilkinson - LHCb-2005-066.

[12] For the latest measurements of δ_D see S.Blusk's talk at ICHEP 2006, session 8, 27.07.2006 $D^0 \rightarrow K^-\pi^+$, Cabibbo-allowed and Cabibbo-doubly-suppressed (S. Blusk for the CLEO-c collaboration).

[13] γ fitted results using $B^+ \rightarrow D^0 K^{*+}$ in the UTFit http://utfit.roma1.infn.it/gamma/ckm-gamma.html

[14] Measuring γ with $B^0 \rightarrow D^0 K^{*0}$ at BABAR, S. Pruvot, M.H. Shune, V. Sordini, A. Stocchi - hep-ph/0703292